# CHAPTER 2

# MONITORING METHODOLOGIES

Visibility is reduced by the presence of aerosols, which are mixtures of fine particles in the air. In order to develop reasonable plans to maintain a given visibility level, we need to know the component species in these aerosols, their sources, their amounts, and their separate effects upon the visibility. Thus, monitoring of protected visibility areas denoted Class I by the Clean Air Act has been on the two parallel fronts of 1) monitoring the composition of the aerosols in these areas, and 2) monitoring the visibility in these areas. These two tasks are performed by the aerosol and visibility monitoring networks of IMPROVE.

The aerosol monitoring network has been operational since spring 1988. The visibility monitoring network coincides with this time frame, and a number of sites go back as far as 1986. This report deals with the first three full years of aerosol data, from spring 1988 through winter 1990/1991.

## 2.1 Aerosol Monitoring Network

The aerosol network is managed by scientists at the University of California at Davis (UCD), according to protocols of aerosol sampling and analysis established by them to meet the needs mentioned in the preceding paragraph. These protocols must therefore meet two goals that are quite independent and sometimes in conflict: 1) determination of not only the aggregate aerosol mass but also the masses of its major constituents, to aid in explaining changes in visibility; and 2) determination, within the smallest possible detection limits, of elements that can act as tracer species to aid in establishing the sources of those constituent particles, natural and man made, that degrade visibility. Finally, the accuracy and precision of all measurements must be assured through strict validation procedures involving continuous, independent field comparisons (of some species) using widely divergent techniques.

The standard IMPROVE sampling module, shown in Figure 2.1, is a filter sampler consisting of the following: 1) an inlet; 2) a cyclone to provide a particle size cutoff based on the flow rate; 3) alternate collection filters, housed in cassettes in the flow path, with each filter followed by a flow on/off solenoid switch; 4) a critical orifice set to provide the proper flow rate for the desired particle size cutoff; and 5) a vacuum pump which produces the flow. The flow rate is monitored by two independent gauges, a magnehelic and a small gauge, which measure the pressure drop due to the flow, across the cyclone and the filter, respectively. Sampling is performed in two 24-hour periods per week.

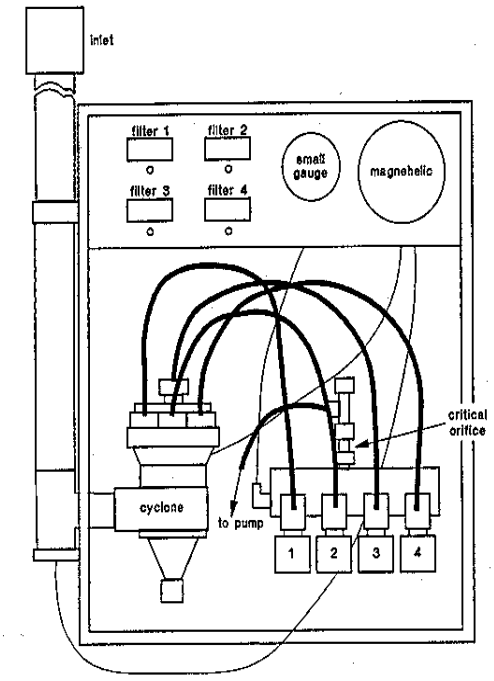


Figure 2.1 Schematic of fine particle aerosol sampling module.

## 2.1.1 Aerosol Sampling Protocol

In order to meet IMPROVE's disparate goals, a basic protocol has been established which calls for four independent sampling modules at each site. Three (denoted A,B and C) are fine particle samplers, with cyclone systems operated at a flow rate of 22.7 liters/minute, which collect particles up to 2.5 µm in diameter. The fourth (D) is a $PM_{10}$ collector, using an 18.9 liter/minute system that collects particles up to 10 µm. Each module is optimized for its specific purpose and matched to its analytical protocols as follows:

| MODULE | FILTER(S) | MEASURED VARIABLES |
|---|---|---|
| A (≤2.5ìm) | 25mm stretched Teflon | Fine Mass, absorption, H, Na to U (PIXE), (H,Li,Be,B,C,N,O) |
| B (≤2.5ìm) | Nitric acid denuder + 25mm Nylasorb filter | $NO_3^-$,$NO_2^-$,$Cl^-$,$SO_4^{2-}$ (Ion Chromatography) |
| C (≤2.5ìm) | Tandem, pre-fired quartz filters | Organic Carbon, Elemental Carbon |
| D/S (≤10ìm) | 25mm stretched Teflon, Impregnated quartz | Total Mass, $SO_2$ Gas(IC) |

It is often convenient to consider a particular module, its associated filter and the variables measured off that filter, as constituting a particular channel of measurement (e.g., "the Channel A filter" or "the Channel C carbon measurement"). The following paragraphs describe the measurements performed on the IMPROVE samples in each of the channels.

Gravimetric mass (Channel A fine mass, Channel D total mass) is measured as the difference between weighing of the filters before and after sampling, using an electromicrobalance.

The Channel A Teflon filters are analyzed for sulfur and other elements by Particle Induced X-ray Emission (PIXE), and simultaneously for hydrogen by Proton Elastic Scattering Analysis (PESA). Both PIXE and PESA involve subjecting the collected aerosol sample to a beam of 4.5 MeV protons, in vacuum, at the UCD cyclotron. In PIXE, each element present in the sample is induced by the proton beam to emit x-rays whose energy is characteristic of the element, and whose number is proportional to the mass of the element. In PESA, the protons in the cyclotron beam which are elastically scattered through a given angle ($30^{\circ}$) by the hydrogen atoms in the sample are also easily discriminated and counted, to give an accurate measure of the amount of hydrogen.

The coefficient of light absorption for fine particles, $b_{abs}$, is also determined from the Channel A Teflon filters using a Laser Integrating Plate Method (LIPM). This involves direct measurement of the absorption of a laser beam by a sample, over the area of the sample. To obtain an ambient $b_{abs}$ value, the LIPM measurement must be corrected both for "shadowing" of some of the particles by others, due to the thickness of the sample, and for scattering effects. The LIPM measurement and its corrections are described more fully in Section 2.1.2.

The Channel B nylon filters are analyzed by Ion Chromatography (IC) for sulfate and nitrate ions, from which the sulfate and nitrate compounds are estimated. A sample is prepared for IC analysis by desorption of the collected material in 15 ml of an aqueous solution of sodium carbonate. This solution is applied to strips of filter paper and allowed to dry, and the various ion species are separated in the standard way according to their solubilities, by suspending the strips over a solvent and allowing it to pass up through the paper by capillary action. Ambient gaseous nitric acid ($HNO_3$) is subject to adsorption by the nylon filter and subsequent transformation to the solid nitrate form, which would bias measurements of the latter. Therefore, a gas denuder, consisting of a set of concentric cylindrical aluminum sheets coated with potassium carbonate ($K_2CO_3$), is placed in the Channel B inlet to remove $HNO_3$ before collection. (This denuder also removes $SO_2$ gas, which could possibly interact with collected particles and contribute falsely to the particulate sulfate measurement. The possibility of such a sulfate artifact, in either Channel A or Channel B, is a particular validation question which has arisen and is discussed in Section 4.1 and in Appendix B.)

The Channel C quartz filters are analyzed by Thermal Optical Reflectance (TOR) Combustion for organic and elemental carbon. A second quartz filter behind the first is used in estimating the artifact due to adsorption of organic gases. TOR involves: (1) heating a sample through a series of temperature increases or steps (in a pure Helium atmosphere to which oxygen is added in the later stages to enable the volatilization of elemental carbon); (2) converting the carbon evolved at each step into $CO_2$, using an oxidizer ($MnO_2$ at 912 $^{o}C$); and (3) reducing the $CO_2$ to

methane, which is then quantified by passage through a flame ionization detector. Figure 2.2 is a graphical portrayal of the TOR process. Over the midrange of the TOR heating (between about 130 $^{o}$C and 550 $^{o}$C), charring of the sample occurs, due to pyrolysis of organic particles; this is monitored as a decrease in the reflectance from the sample surface. When the reflectance reaches a minimum, 2% oxygen is added to the atmosphere. This allows the elemental carbon in the sample, including the char produced by pyrolysis of organic matter, to oxidize; and the reflectance of the sample increases as the char is removed. All carbon measured up to the point where the reflectance reattains its initial value is interpreted as organic carbon. Carbon evolved beyond this point is reported as elemental carbon. Overall, the peaks in the carbon evolution from the sample (Figure 2.2) are conveniently divided into low- and high-temperature organic, and low- and high-temperature elemental, carbon--respectively OCLT, OCHT, ECLT AND ECHT. Organic carbon (OC) is the sum of the reported OCLT and OCHT. Elemental carbon is also known as light-absorbing carbon (LAC), and is the sum of ECLT and ECHT:

$$OC=OCLT+OCHT \qquad (2.1)$$

$$LAC=ECLT+ECHT \qquad (2.2)$$

The S, or secondary Channel D, filters are analyzed by ion chromatography for $SO_2$ gas. These filters are quartz impregnated with $K_2CO_3$, which changes $SO_2$ to solid $K_2SO_4$ on the filter. The $K_2SO_4$ is then analyzed by IC for $SO_4^{2-}$ to give a measure of the original gas.

## 2.1.2 Uncertainties

The amount of each aerosol species in a 24-hour sample is reported as an average ambient concentration, which is the collected mass of the species divided by the volume of air sampled. Both mass measurements and volume calculations have their uncertainties, as discussed below.

Uncertainty in an aerosol species measurement may be given in terms of a minimum detectable limit (MDL) for the species. The MDL is defined, for every species, in terms of the observed standard deviation $\sigma_{FB}$ in the measurement of the species off of supposedly blank filters (ones not subjected to sample flow, including laboratory controls and field blanks).

The general equation for the concentration ($C$) of a given species is

$$C=(M-A)/V \qquad (2.3)$$

where $M$ is the measured mass of the species, $V$ is the volume of air sampled, and $A$ is the artifactual mass (discussed below). The uncertainty in a measured concentration is the quadratic sum (the square root of the sum of the squares) of the uncertainties in $M$, $A$, and $V$: respectively, the analytical uncertainty, the artifact uncertainty and the volume uncertainty.

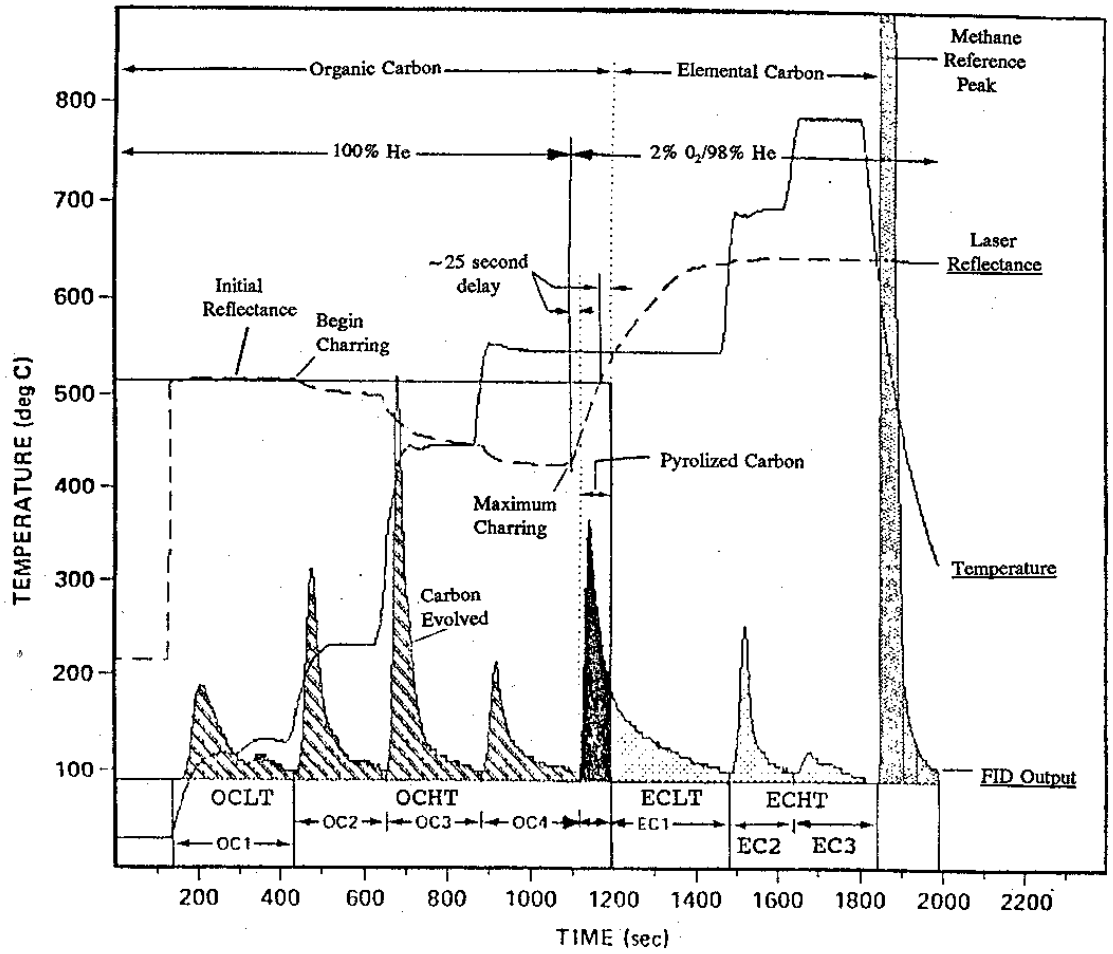


Figure 2.2 Time development of TOR carbon analysis. Area of shaded peaks are the amount of carbon evolved at successive steps in temperature (stepped solid line). Pyrolysis changes some organics to elemental carbon (charring), decreasing the sample reflectance (broken line); reattainment of initial reflectance marks the end of the pyrolyzed organic carbon. There is a 25 second delay between the sample chamber and the detector. (Modified after Chow et al., 1992.)

The artifact A may be positive, due to accrued nonaerosol mass, or negative, due to a failure to collect some portion of the considered aerosol species or to volatilization of particles that are collected (especially nitrates). The artifact may be produced by contamination in the filter material, by handling, and/or by adsorption of gases during collection. It is determined from secondary quartz filters for the Channel C carbon, and from designated field blank filters for all other measurements. These secondary or field blank measurements also contribute to the analytical uncertainty, particularly when the artifact is negligible.

The artifact has been found to be negligible for all measurements off the Teflon filters (Channels A and D), including PIXE, PESA, LIPM absorption, gravimetric analysis, and $SO_2$. General uncertainty considerations for the sample volume and the measured aerosol species follow.

Volume--The volume is the product of the average flow rate and the sample duration. The average flow rate is calculated from the magnehelic and small gauge readings taken at the beginning and end of the sampling period. The fractional uncertainty in volume equals the fractional uncertainty in flow rate, since the sample duration is well defined. The precision of the magnehelic and small gauge flow measurement system is as good as the precision of most audit devices. At present, the best estimate of internal precision of average flow rate is that it is better than 1%; and the best estimate of total uncertainty is that it is better than 3%. All calculations are based on a volume uncertainty of 3%.

Gravimetric Mass--The uncertainty in mass concentration is

$$\sigma_C = \left[ \left( \sigma_{FB} / V \right)^2 + \left( f_V C \right)^2 \right]^{1/2} \qquad (2.4)$$

where $\sigma_{FB}$ is the standard deviation of the mass measured in the controls and field blanks, $V$ is volume, and $f_v$ is the fractional uncertainty in volume. The artifact is generally negligible, and the MDL ($=2\sigma_{FB}/V$), which is due to analytic uncertainty alone, is a constant 300 ng/m$^3$. In the third year, an organic artifact is associated with a small proportion (about 7%) of the Teflon filters being used. This artifact is discussed in Section 4.3 of this report.

PIXE and PESA Analysis--A PIXE measurement is performed by counting the x-rays in the element's spectral peak, normalizing to the number of protons passing through, and calibrating the system using known elemental standards. A background is subtracted, using the spectrum of a blank Teflon filter. PESA works the same way as PIXE, only counting the protons scattered by hydrogen rather than the x-rays emitted by it.

The artifact concentrations for the elements measured by PIXE and PESA are zero. The uncertainty in the concentration is thus the square root of the sum of the squares of the analytical uncertainties and the volume uncertainty. The analytical uncertainties are the uncertainty in calibration, which is about 4% over the long term, and the statistical uncertainty, which is

proportional to the square root of the number of counts in the spectral peak. The 3% volume uncertainty and the 4% PIXE/PESA calibration uncertainty combine to give an uncertainty of 5%; and the total uncertainty is thus 5% plus counting statistics (again, combined quadratically).

A PIXE or PESA measurement actually determines the areal density of a given element, which is the mass of the element per unit area of the sample. To determine concentration, the areal density is multiplied by *SA/V*, where *SA* is the sample area on the filter. PIXE/PESA analysis can be performed on deposit areas smaller than 2 $cm^2$, so some filters are masked to limit the deposit area, thus concentrating the particles and reducing the minimum detectable limits of the tracer elements to as low as 0.05 $ng/m^3$.

Optical Absorption--The coefficient of absorption, $b_{abs}$, for the particles on the Channel A filter, depends on the initial and final LIPM measurements, the volume, and the filter sample area. A LIPM measurement gives the intensity of laser light transmitted through a sample (through a blank filter for the initial measurement). The intensity measurement is basically related to $b_{abs}$ through the relation

$$L_f = L_i e^{-b_{abs} t} \qquad (2.5)$$

or

$$b_{abs} = (1/t)\ln(L_i / L_f) \qquad (2.6)$$

where $t$ is the thickness of the sample, and $L_i$ and $L_f$ are the LIPM measurements before and after particle collection, respectively. The $b_{abs}$ value thus obtained must be corrected for the portion of light loss that is due to scattering by the particles rather than absorption. This correction, amounting to a reduction of 3%, has been determined by comparing the LIPM measurements with those using Laser Integrating Sphere Analysis (LISA), pictured in Figure 2.3. (In LISA, the absorption by the sample is basically the incident light energy minus the sum of the total reflected and transmitted energies over all scattering angles, as collected by the sphere.) Also, particles on the filter overlay and thus shadow one another in the measurement; so it is necessary to divide the measured coefficient by a factor $R$ that depends on the areal density of the particles on the filter, to obtain the true value of $b_{abs}$ for the atmosphere. (The function of $R$ has been established experimentally by studying the variation of $b_{abs}$ with areal density, as shown in Figure 2.4.) The coefficient of absorption in the atmosphere is thus given by

$$b_{abs} = (SA/V)\ln(L_i / L_f)(0.97 / R) \qquad (2.7)$$

where $SA/V = 1/t$ is the sample area divided by the sample air volume. The average uncertainty in $b_{abs}$ is 13%.

Ion Chromatography--IC analysis of field blanks indicates that there is artifact formation during the period in the cassettes in the sampling module. The standard deviation in the measurement off the field blanks provides an estimate of the artifact uncertainty. The analytical

uncertainty, based on data from replicate samples, is not a constant, but varies directly with the measured value. The uncertainty in concentration $C$ is given by:

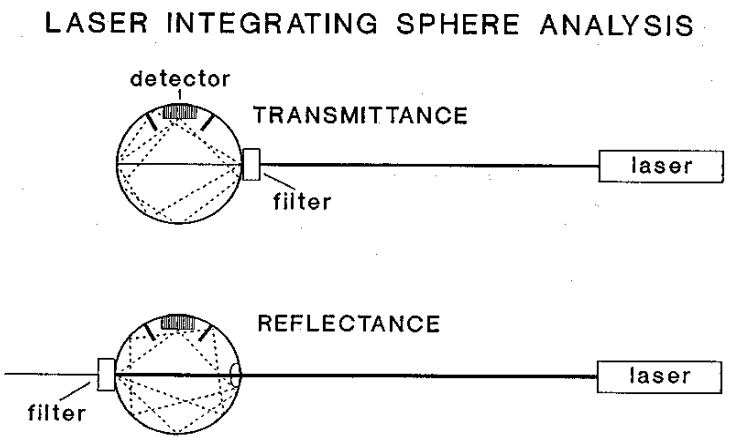


Figure 2.3 LISA configuration. Transmitted energy $E_T$ is measured with filter sample on front side of sphere; reflected energy $E_R$, with sample on back side. Absorption is then $E_A = E - (E_T + E_R)$, where $E$ is the energy in the incident beam. Coefficient of absorption is $\alpha = E_A/E = 1 - (T+R)$, with $T$=transmittance and $R$=reflectance.

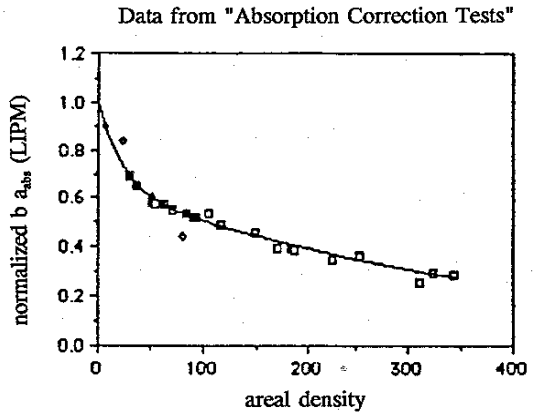


Figure 2.4 Variation of $b_{abs}$ with areal density, $\gamma$. Normalized $b_{abs}$ is $R(\gamma)$, where $R = ke^{(\gamma/A)} + (1-k)e^{(\gamma/B)}$, with constants $k$, $A$, $B$.

$$\sigma_C = \left[ (f_A M / V)^2 + (\sigma_{FB} / V)^2 + (f_V C)^2 \right]^{1/2} \qquad (2.8)$$

where $M$ is the mass measured by the ion analysis and $f_A$ is the fractional analytic uncertainty. The MDL is equal to twice the uncertainty measured on field blanks: MDL = $2(\sigma_{FB}/V)$ .

Carbon Analysis--Artifacts in the carbon measurements are based on measurements on secondary quartz filters placed behind the primary C filters in the sample flow. Organic carbon artifact is caused by contamination in the filter material, by contact with the cassette, and by the adsorption of organic gases during collection. The quartz filters are pre-fired to eliminate filter contamination; however, this process itself may produce surface sites on the filter material that will enhance later organic adsorption. Elemental carbon artifact is caused by contamination in the filter material and by contact with the cassette. (See Chapter 4, "Validation," on carbon measurements.) Uncertainties associated with the TOR analysis are shown in Table 2.1.

The carbon artifacts are constants, and are consistent with their values as derived from designated field blanks. Unfortunately, these carbon artifacts appear to be too large, since approximately 21% of the carbon measurements for the first two years were negative, and comparisons with other measurements give a negative carbon intercept. The reasons for this problem have not yet been determined, so correcting these negatives as yet simply involves adding a constant to the reported carbon concentrations. In this report, carbon corrections have been performed by finding the minimum concentration for each season at each site, and subtracting this, if it is negative, from every concentration in that season (thus adding a positive number to the concentrations). For the comparisons performed for this report, involving one or another sum of the individually reported varieties of carbon (for example, finding the total organic carbon from the reported high- and low-temperature forms), the appropriate sum has been taken before applying the correction.

Overall percentage uncertainties for the average concentrations of measured species are given in Table 2.2. The uncertainties of the composite variables (cf. Chapter 3 for their definitions) are estimated by quadratically adding the uncertainties of the components, assuming those uncertainties are independent. Since this is not quite valid, the uncertainties for composites formed by adding (SOIL, OMC, LAC) may be slightly larger than as given in Table 2.2 (5% for SOIL, rather than 4%, for example). The composite formed by subtraction (OMH) may have a slightly smaller uncertainty than reported.

The measured concentrations may be less than the MDL of the analytical system used, and therefore not quantifiable. This is generally not a problem with the ion chromatography and carbon combustion variables, because the presence of artifact means that some material is always measured. The problem for these variables is that the concentrations after removing artifact may have a large fractional uncertainty, and for this reason not be statistically reliable. For the $PM_{10}$ mass and the Channel A variables, the situation is different. Here there is no significant artifact, and the concentration may be so low that nothing can be determined because of statistical noise. In such a case, the concentration reported is just the MDL for the given species. When calculating averages and composite variables, when the value is below the MDL, it is dropped

Table 2.1. Specifications of the DRI Thermal/Optical Reflectance Carbon Analyzer.

| SUBJECT | SPECIFICATION |
|---|---|
| Sample Requirements | Substrate: Quartz-fiber filter, Pallflex 2500QAT-UP or equivalent |
| | Substrate pretreatment: Pre-fired at 900 $^{o}$C for at least 3 hours (before sampling) |
| | Sample size: 0.5 $cm^2$ punch (uniform deposit) |
| | Sample storage: Store below 4 $^{o}$C |
| Analysis Time | 880 to 4,890 seconds (15 to 82 minutes) |
| Measurement Range | 0.2 to 750 ìg carbon/$cm^2$ |
| Detection Limit | 0.2 ìg carbon/$cm^2$ |
| FID Precision | 0.1% of full scale |
| Reflectance Signal Precision | 0.2% of full scale |
| Sample Oven Temperature Precision | ± 10 $^{o}$C at temperatures < 450 $^{o}$C |
| | ± 3 $^{o}$C at temperatures ≥ 450 $^{o}$C |
| Oxidation Oven Temperature | 912 ± 5$^{o}$C |
| Methanator Oven Temperature | 550 ± 5$^{o}$C |
| Lower Quantifiable Limits | Organic carbon: 0.5 to 1.0 ìg carbon/$cm^2$ |
| | Elemental carbon: 0.0 to 0.2 ìm carbon/$cm^2$ |
| | Carbonate carbon: 0.0 to 0.4 ìg carbon/$cm^2$ |
| Total Carbon Accuracy | ±5% |
| Total Carbon Precision | For sample loading < 10 ìg carbon/$cm^2$: ±0.5 ìg carbon/$cm^2$ |
| | For sample loading ≥ 10 ìg carbon/$cm^2$: ±3% |
| OC/EC Split Precision: | 5% of the total carbon measurement |
| OC/EC Split Accuracy | To be determined* |

* Probably 10% of the total carbon, by inference from the similar DRI instrument (Johnson et al., 1981).

Table 2.2 Precisions for average concentration of measured and composite variables.

| | | | | | | | |
|---|---|---|---|---|---|---|---|
| MASS | 4% | Fe | 5% | Pb | 14% | NHSO | 6% |
| $PM_{10}$ | 4% | Mn | 25% | Na | 10% | LAC | 25% |
| H | 6% | V | 30% | $CL^-$ | 39% | OMC | 18% |
| S | 5% | Ni | 14% | OCLT | 80% | OMH | 12% |
| $SO_2$ | 9% | Cu | 11% | OCHT | 25% | SOIL | 4% |
| Si | 6% | Zn | 7% | ECLT | 21% | RCMC | 7% |
| K | 6% | As | 16% | ECHT | 81% | RCMA | 5% |
| Ca | 6% | Se | 20% | $b_{abs}$ | 13% | | |
| Ti | 15% | Br | 11% | KNON | 14% | | |

and reported as simply one half of the MDL. And in such a case for a composite variable, one half the MDL is also used as the uncertainty.

## 2.2 Visibility Monitoring Network

The NPS Visibility Monitoring Network currently consists of 20 IMPROVE and IMPROVE Protocol sites. Each site contains an Optec, Inc., LPV-2 long path transmissometer system, a Handar data collection platform (DCP), a Handar Air Temperature/Relative Humidity sensor and a Primeline two-pen strip chart recorder. The data collection platform automatically transfers collected data through the GOES satellite to the visibility network manager, Air Resource Specialists, Inc.

The transmissometer, shown in Figure 2.5, consists of a transmitter (housing a light source) and a receiver (with light detector). The transmissometer system measures the ambient light loss (or extinction) from the transmitter to the receiver. These two individually-housed components are generally separated by a sight path distance of 0.5 to 10 kilometers, a long path length being required in order to accurately measure extinctions near the Rayleigh limit (which is the extinction due to particle-free, pristine air).

Given the exact amount of light emitted from the light source ($I_0$) and the amount reaching the receiver ($I$), the receiver computer can calculate the atmospheric transmission coefficient, $T$, as the ratio $I/I_0$. (See Equation 2.8 and the discussion of Section 2.2.1.) Given the sight path distance $r$, $T$ can be converted to the atmospheric extinction coefficient $b_{ext}$ according to

$$b_{ext} = -\ln(T)/r \qquad (2.9)$$

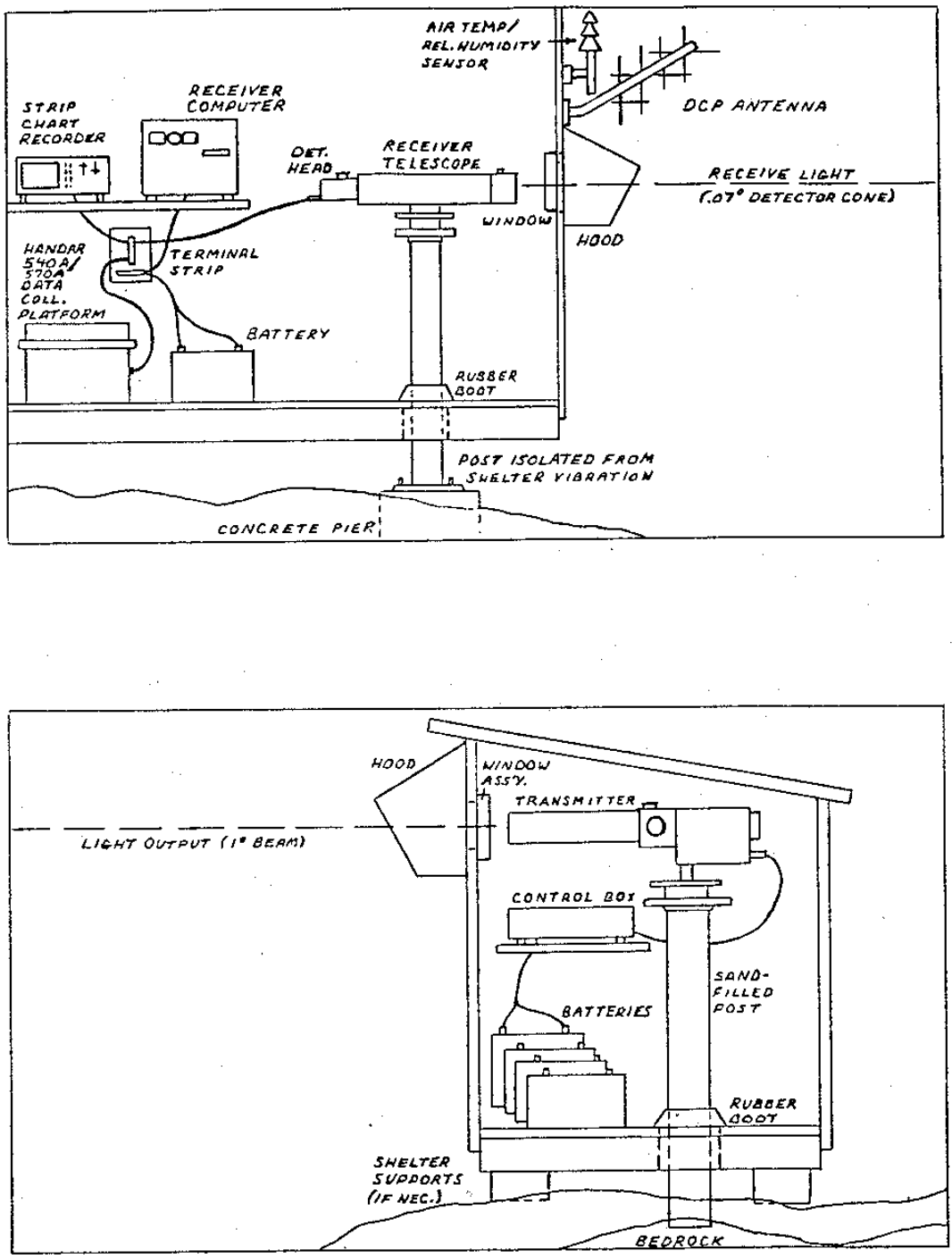


Figure 2.5 Transmissometer receiver (top) and transmitter (bottom).

A standard visual range may also be defined, as that distance over which the transmission coefficient is reduced to 2%, which from Equation 2.9 becomes

$$SVR = 3.91 / b_{ext} \qquad (2.10)$$

The transmission $T$ is calculated for each hour, based on a ten-minute sample (which is itself composed of ten successive one-minute samples over a ten minute period). Temperature and relative humidity averages are simultaneously collected. The strip chart recorder allows the site operator to verify system operational performance, and provides data backup in case of DCP or GOES system failure.

## 2.2.1 Uncertainties

Transmissometer--The basic equation used to calculate path transmission is:

$$T = I_r / \left(F_{lamp} \cdot I_{cal}\right) \qquad (2.11)$$

where: $I_r$ = Intensity of light measured at distance $r$,
$I_{cal}$ = Calibration value of transmissometer,
$F_{lamp}$ = Variability function of lamp output.

The relative uncertainty ($U_x$) of any measured quantity $X$ is:

$$U_x = \sigma_x / \overline{X} \qquad (2.12)$$

where = arithmetic mean of all $X$ measurements, and $\sigma_x$= precision (S.D.) of measurements of $X$. The relative uncertainty of the transmission is calculated from the relative uncertainties of the measured variables as:

$$U_T = \left(U_{Ir}^2 + U_{Ical}^2 + U_{lamp}^2\right)^{1/2} \qquad (2.13)$$

$I_{cal}$ is the value that would be measured by the transmissometer detector if the atmospheric path were a vacuum. $I_{cal}$ incorporates the path distance, the transmission of all windows in the path, and the size of the working aperture used, according to

$$I_{cal} = \left(CP / WP\right)^2 \left(WG / CG\right)^2 \left(WA / CA\right)^2 \left(WT\right)\left(1 / FT\right)\left(1 / T\right)\left(CR\right) \qquad (2.14)$$

and the relative uncertainty is

$$U_{Ical} = \left(2U_{CP}^2 + 2U_{WP}^2 + 2U_{WG}^2 + 2U_{CG}^2 + 2U_{WA}^2 + 2U_{CA}^2 + U_{WT}^2 + U_{FT}^2 + U_{CR}^2\right)^{1/2} \quad (2.15)$$

The parameters in Equations (2.14) and (2.15) are given in Table 2.3. Path distances are measured using a laser range finder. Apertures are measured with a precision micrometer. Gain settings are measured with a precision voltmeter. Window and neutral density filter transmittances are measured with a reference transmissometer by differencing techniques; thus, they do not require absolute calibration. The standard deviation of the raw readings (CR) are calculated at each calibration. From the typical values given in Table 2.3, the predicted relative uncertainty in $I_{cal}$ is $U_{Ical}$=0.008. Experimentally, $U_{Ir}$ is a function of the extinction of the path. Typically, for weather-affected data, $U_{Ir}$=0.15, otherwise, $U_{Ir}$=0.006.

The transmissometer lamp brightness is continually adjusted by an optical feedback circuit. However, the lamp brightness still increases with usage, typically by 2% per 500 hours of lamp life, according to precise measurements. $U_{lamp}$ is simply the precision of those measurements, which is 0.002. The transmissometer data is corrected to fully account for the time drift.

Table 2.3 Transmissometer parameters.

| | Parameter | Value | Precision | Relative Uncertainty |
|---|---|---|---|---|
| CP | Calibration Path | 0.3 km | $1 \times 10^{-6}$ km | $3.3 \times 10^{-6}$ |
| WP | Working Path | 5.0 km | $1 \times 10^{-6}$ km | $2.0 \times 10^{-7}$ |
| CG | Calibration Gain | 100 km | $1 \times 10^{-2}$ km | $1.0 \times 10^{-4}$ |
| WG | Working Gain | 500 km | $1 \times 10^{-2}$ km | $2.0 \times 10^{-5}$ |
| CA | Calibration Aperture | 100 mm | $1 \times 10^{-2}$ mm | $1.0 \times 10^{-4}$ |
| WA | Working Aperture | 110 mm | $1 \times 10^{-2}$ mm | $9.1 \times 10^{-5}$ |
| WT | Window Transmission | 0.810 mm | 0.001 mm | $1.2 \times 10^{-3}$ |
| FT | NDF Transmission | 0.274 mm | 0.001 mm | $3.6 \times 10^{-3}$ |
| T | CP Transmission | 0.975 mm | 0.005 mm | $5.1 \times 10^{-3}$ |
| CR | Raw Readings | 900 mm | 4.5 mm | $5.0 \times 10^{-3}$ |

From the above analysis, typical values for the relative uncertainty in path transmission $T$, for each 10-minute transmission measurement, can be calculated using Equation (2.13):

$U_T$ = 0.01, with no optical interference,
$U_T$ = 0.20, with optical interference.

The extinction over the distance $r$ is given by Equation 2.16:

$$b_{ext} = -\ln(T)/r \qquad (2.16)$$

and since $r$ is measured to an extremely high precision with a laser range finder, the uncertainty in $b_{ext}$ is:

$$\sigma_{bext} = 0.01/(10km) = 0.01/(0.01Mm) = 1Mm^{-1} \qquad (2.17)$$

For $r$ between 0.5 and 10 kilometers, then, and $b_{ext}$ given in $Mm^{-1}$, the minimum uncertainty in $b_{ext}$ is

$$\sigma_{bext} = 0.01/(10km) = 0.01/(0.01Mm) = 1Mm^{-1} \qquad (2.18)$$

so that $b_{ext}$ should be reported only to the nearest $Mm^{-1}$ (as done in Chapter 7). In addition, a bias in $b_{ext}$ can occur if the transmission of the windows is altered, by staining, pitting, collecting dirt, fogging, or breakage. This bias is of the same form as that of $\sigma_{bext}$ above, that is:

bias = (relative change in window transmission)/$r$.

The uncertainties and limits for air temperature and relative humidity are obtained form the manufacturer's literature:

$U_{temp}$ = 1°C
$U_{RH}$ = 5%, for Handar sensors
2%, for Rotronics sensors
Maximum temperature = 60°C
Minimum temperature = -50°C
Maximum rel. humid. = 100%
Minimum rel. humid. = 0%

Figure 2.6 is a scatter plot (with one-to-one line indicated) of hourly extinction data collected by two short-path transmissometers during a summer 1991 study at Shenandoah National Park (Molenar et al., 1992). Figure 2.7 is a similar plot of data collected by two long-path transmissometers during a similar intercomparison study at Tonto National Monument in Arizona. Both figures indicate the extremely high precision of transmissometers to replicate extinction measurements when operating over identical paths. Figure 2.8 is a scatter plot of extinction by short-path vs. long-path transmissometers during the Shenandoah summer 1991 study. The correlation is again outstanding. Analysis of the extinction data from the short- and long-path transmissometers, shown in Table. 2.4, indicate that the predicted uncertainties ($U_T$) of 0.01 and 0.20, for weather and nonweather affected data, respectively, agree very well with the actual calculated uncertainties.

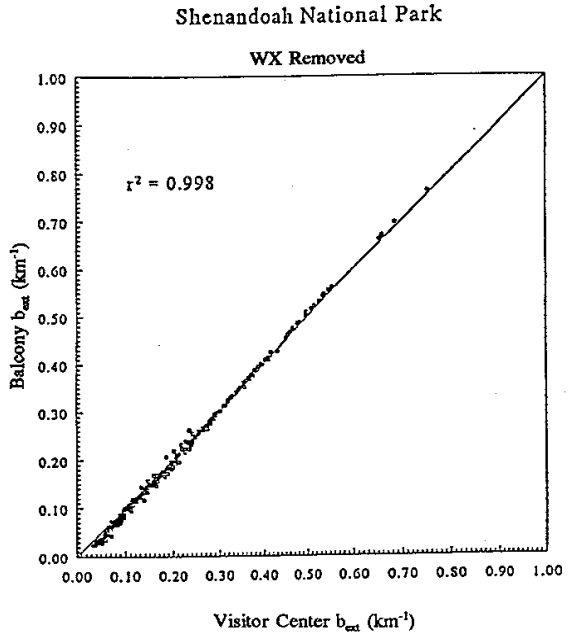


Figure 2.6 Comparison of $b_{ext}$ measured by two transmissometers operating side-by-side over a short path (0.67 km). (Molenar et al., 1992)

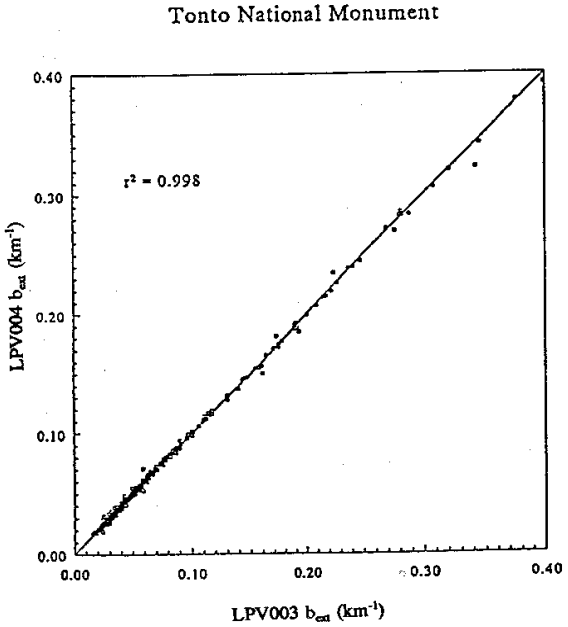


Figure 2.7 Comparison of $b_{ext}$ measured by two transmissometers operating side-by-side over a long path (7.2 km). (Molenar et al., 1992)

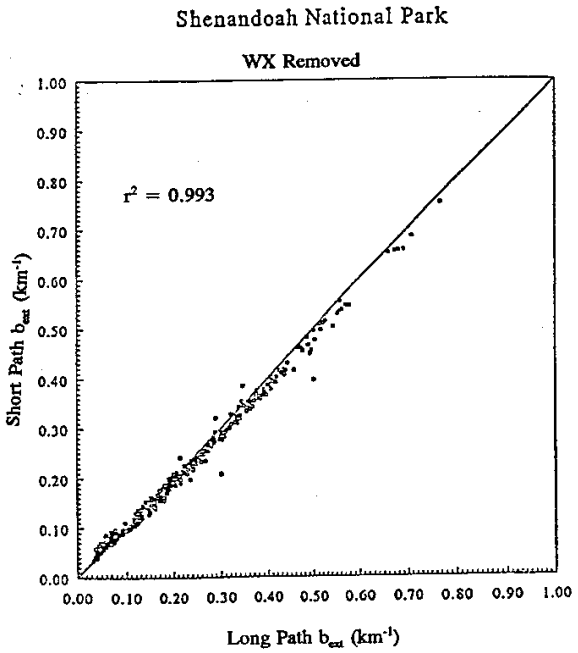


Figure 2.8 Comparison of $b_{ext}$ measured by two transmissometers, one operating over a short path (0.67 km), the other over a long path (1.41 km). (Molenar et al., 1992)

Table 2.4 Calculated $U_T$, Shenandoah summer 1991 study. (Molenar et al., 1992.)

| | **Uncertainty $U_T$** | |
|---|---|---|
| **Path** | **Weather** | **No Weather** |
| 1.41 km | 0.14 $km^{-1}$ | 0.007 $km^{-1}$ |
| 0.67 km | 0.30 $km^{-1}$ | 0.015 $km^{-1}$ |

RH Sensor--The importance of the effect of relative humidity (RH) on the scattering properties of aerosols cannot be overstated. Accurate RH measurements are mandatory for a proper understanding and comparison of ambient optical measurements and ambient aerosol extinction apportionments. Recent advances in the design and manufacture of low-power thin film capacitive RH sensors provide the means to obtain accurate measurements of RH. Sensors of this type have historically been plagued by nonlinear response, hysteresis, creep and instability, particularly at high humidity levels.

Ambient temperature and relative humidity measurements were made with three RH sensor systems during the summer 1991 Shenandoah study. The first was an old-style capacitive sensor, a

Campbell 207 essentially the same as the Handar RH sensor used up to that point in IMPROVE. The second was a new model by Rotronics (model MP-100MF). This sensor featured temperature compensation and a new polymer engineered to minimize hysteresis and creep. The third system was an Assman model 5230 psychrometer modified for continuous, unattended operation. Modifications included a large water reservoir, type E fine-wire thermocouple affixed to each bulb, and a low-power ventilation fan. Wet and dry bulb temperatures were logged with a Campbell Scientific 21X micrologger equipped with an internal thermocouple reference junction.

Figure 2.9 shows scatter plots comparing the wet/dry bulb standard with the Rotronics and Campbell 207 systems. The Rotronics RH sensor is clearly superior to the Campbell 207, which deviates strongly from the wet/dry bulb system for RH greater than 90%. The RH data for the first three years of IMPROVE aerosol monitoring is from a (Handar) sensor like the Campbell 207, and is suspect above 90% RH; as discussed in the next section, transmissometer data taken when RH is greater than 90% is routinely deleted from the data base. The Rotronics system is now replacing the older system in the IMPROVE visibility monitoring network, which will allow retaining extinction data taken with RH above 90%.

### 2.2.2 Meteorological and Optical Interferences

The transmissometer directly measures the irradiance of a light source after the light has travelled over a finite atmospheric path. The average extinction coefficient of the sight path is calculated from this measurement, and is attributed to the average concentration of atmospheric gases and ambient aerosols along the sight path. The intensity of the light, however, can be modified not only by intervening gases and aerosols, but also by:

- the presence of condensed water vapor in the form of fog, clouds and precipitation along the sight path;
- condensation, frost, snow or ice on the shelter windows;
- reduction in light intensity by insects, birds, animals or vegetation along the sight path, or on the optical surfaces of the instrumentation or shelter windows; or
- fluctuations in light intensity, both positive and negative, due to optical turbulence, beam wander, atmospheric lensing, and miraging caused by variations in the atmospheric optical index of refraction along the sight path.

A major effort was undertaken to develop an algorithm to identify transmissometer extinction data that may be affected by the interferences described above. This algorithm contains five major tests:

1) Relative Humidity--The transmissometer measurement is flagged as having a possible interference when the relative humidity measured at the receiver is greater than 90%. This is because inferring the precise meteorological conditions along the sight path from a single point measurement is very difficult, and when RH is above 90% at one end of the path, small random

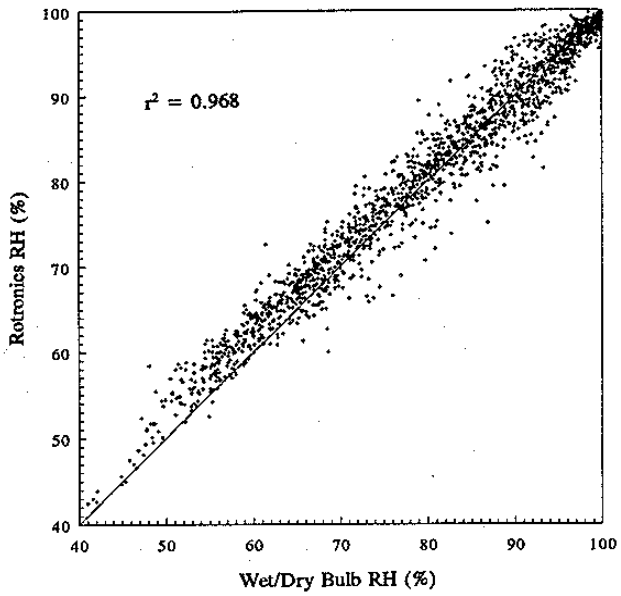


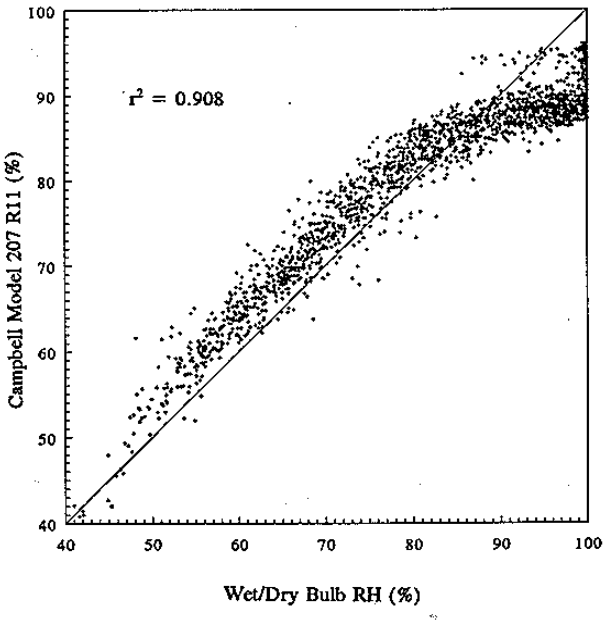


Figure 2.9 Comparisons of Rotronics MP-100MF and Campbell 207 RH sensors against Wet/Dry Bulb standard. (Molenar et al., 1992)

temperature or absolute humidity fluctuations along the path can lead to condensation of water vapor, causing meteorological interference to the transmissometer beam.

2) Maximum Extinction--Transmissometer measurements of $b_{ext}$ greater than a calculated maximum for the sight path are flagged. This maximum corresponds to a 2% transmission for the path, and, based on historical visibility data, this maximum $b_{ext}$ occurs less than 1% of the time. Beyond this maximum, it is assumed that meteorological or optical interferences are involved, not ambient aerosols.

3) Uncertainty Threshold--The normal procedure for the transmissometer is to take ten one-minute measurements of transmissometer irradiance each hour, and report the average and standard deviation of the ten values. In remote, rural areas the ambient aerosol concentration typically varies quite slowly, with time constants on the order of a few hours, not minutes. Thus, any measurement with a standard deviation, or uncertainty, above a selected threshold implies variation beyond that due to ambient aerosols, and is flagged as interference.

4) Rate of Change of Extinction--Transmissometer data collected before September 1, 1990 did not include standard deviation of measured irradiance values. For this data, periods of interferences were identified by comparing the hourly extinction to the preceding and succeeding hours, and calculating a rate of change in each direction. The hourly $b_{ext}$ value is flagged as being affected by interferences when this rate of change exceeds an assigned delta threshold.

5) Isolated Data Points--After the above four thresholds are applied to the hourly extinction data, those data points that are isolated between $b_{ext}$ data that have failed the above thresholds are also flagged as due to interference.